Theory of grating superstructures

N. G. Raphael Broderick* and C. Martijn de Sterke†
School of Physics and Australian Photonics Cooperative Research Centre, Australian Technology Park, Eveleigh, 1430, Australia
(Received 9 October 1996)

We develop the theory of linear and nonlinear grating superstructures, gratings in which the parameters vary periodically with position on the scale of typically about 1 mm. Following earlier work in semiconductors, these have now been written in optical fibers. We develop the theory by introducing a set of *superenvelopes*: envelopes of the usual envelope functions of the grating structure. We show that under very general conditions these superenvelopes satisfy a set of supercoupled mode equations, and that these equations have solitary wave solutions. [S1063-651X(97)11103-5]

PACS number(s): 03.40.Kf, 42.81.Wg, 42.79.Dj

I. INTRODUCTION

Recent developments in grating writing techniques in optical fibers allow for the fabrication of a wide range of nonuniform Bragg gratings [1]. Among the more important designs are superstructure gratings (SSG's) or optical superlattices [2]. These are gratings in which the parameters are periodically modulated with a period of typically 100 μm–1 cm. Using different techniques, a variety of periodic profiles can be fabricated [3–6]. In Fig. 1 we show the variation of the coupling strength κ, which is proportional to the refractive index modulation, with position for a SSG. Note that the strength varies periodically, with a period of 9 mm, and that the repeated profile has a triangular shape. The periodic modulation of the SSG results in a comblike reflection spectrum with the various peaks, the ''Rowland ghosts,'' [7] being closely spaced in frequency.

In semiconductor geometries, SSG's have been used in tuneable distributed feedback lasers [8,9], something which has also recently been achieved in optical fibers [4]. In optical fibers, SSG's have also been used as multichannel dispersion compensators in wavelength division multiplexing systems [10]. It should be mentioned that sometimes an SSG is written unintentionally if the phase mask used to write a *uniform* grating has periodic *stitching errors* [6].

Of course the properties of SSG's can be found by solving the relevant coupled mode equations numerically, but this does not give much physical insight. Therefore, in the applications mentioned above the SSG has often been assumed to be ''weak'' allowing a Fourier description to be used [8]. In this description the different reflection peaks are well separated, and the peak reflectivity of the jth peak is given by $\tanh^2(\kappa_j L)$, where L is the length of the grating and κ_j is the strength of the jth component in the Fourier decomposition of the SSG.

The Fourier method mentioned above is similar to the standard coupled mode analysis of uniform Bragg gratings [11], in which only a single Fourier coefficient of the refractive index profile is included. But this approach fails when the grating is too deep, i.e., when the refractive index modulation depth is too large [12,13]. Similarly, the Fourier description is valid for weak SSG's, but it fails when the SSG is sufficiently deep. We see below that deep superstructures can easily be obtained in fiber geometries, even though the gratings themselves are shallow; then an alternative to the Fourier description must be used for the quantitative description of an SSG.

Recently a convenient method was developed by de Sterke *et al.* [12,13] to treat deep Bragg gratings. It leads to a set of coupled mode equations which are similar to those which follow from conventional coupled mode theory. De Sterke's approach relies on the Bloch functions [14] of the grating and thus a knowledge of the linear properties of the grating is required. We have adapted this approach so that it can be applied to treat deep SSG's; it makes use of the SSG's Bloch functions. We reported on some preliminary results earlier [15,16]. Here we give the full theory and discuss the implications of our results in detail. In our discussion we follow closely the notation of Ref. [13], as many of the results established there carry over to SSG's. Our theory

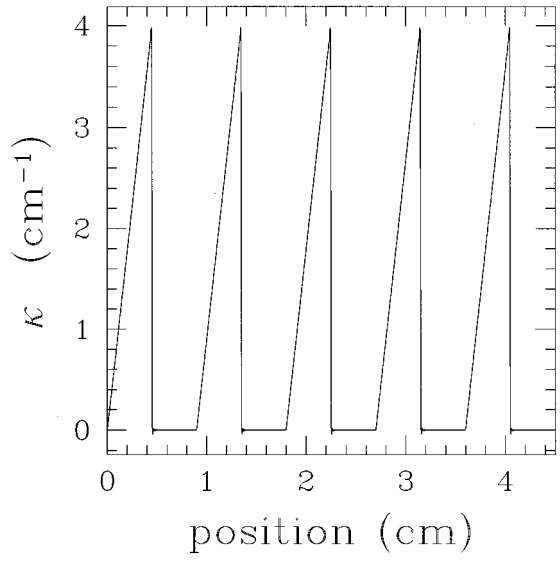

FIG. 1. Coupling coefficient κ as a function of position for a typical SSG. Note that κ is periodic and with a period of 9 mm.

*Present address: Optoelectronic Research Centre, Southampton University, Southampton SO17 1BJ, United Kingdom.
†Fax: (612) 9351 7726. Electronic address: desterke@physics.usyd.edu.au

is also well suited to problems involving optical nonlinearities. This is of particular importance as the first results of high-intensity pulse propagation experiments in SSG's, written in the optical fibers, were recently reported [5].

The outline of this paper is as follows. In Sec. II we present the coupled mode equations for SSG's, and analyze the linear properties of SSG's. In Sec. III we present the evolution equations for the superenvelopes in a nonlinear SSG. We use a one-band approximation, leading to the nonlinear Schrödinger equation (Sec. III A), as well as a two-band approximation (Sec. III B), leading to supercoupled mode equations. Solutions to the supercoupled mode equations are discussed in Sec. IV.

II. COUPLED MODE EQUATIONS

We consider one-dimensional propagation through a grating with a nearly periodic refractive index, i.e. [17],

$$n(x)=n_0+\delta n(x)+\Delta n(x)\cos\left(\frac{2\pi x}{d_0}+\vartheta(x)\right), \tag{1}$$

where δn, Δn, and ϑ are, in principle, all slowly varying functions of position, while n_0 and d_0 are a fixed reference refractive index and period, respectively. Note that the actual period d of the grating may be varied through variation of $\vartheta(x)$. In addition to the spatial dependence in Eq. (1), we take the grating to exhibit a Kerr nonlinearity; the refractive index thus depends on intensity through

$$n(I)=n_l+n^{(2)}I, \tag{2}$$

where I is the intensity and $n^{(2)}$ is the nonlinear refractive index.

In the usual applications, gratings couple light with a wave number around $k_0=\pm\pi/d_0$, to $k_0=\mp\pi/d_0$, i.e., they reflect light with wave number k_0 [11,17]. Defining ω_0 as the frequency at k_0, then for light with a frequency ω such that $\omega\approx\omega_0$, propagating through a Bragg grating, one may approximate the electric field as [17]

$$E(x,t)=\left[E_+(x,t)e^{+i(k_0x+\vartheta/2)}+E_-(x,t)e^{-i(k_0x+\vartheta/2)}\right]\times e^{-i\omega_0t}+\text{c.c.}, \tag{3}$$

where c.c. indicates the complex conjugate, and we have assumed the grating to be shallow. The functions $E_\pm$ are the slowly varying envelopes of the forward and backward propagating modes. With this ansatz for the electric field we can approximate Maxwell's equations by [18,19]

$$+i\frac{\partial E_+}{\partial x}+\frac{i}{v_g}\frac{\partial E_+}{\partial t}+\kappa(x)E_-+\delta(x)E_++2\Gamma|E_-|^2E_++\Gamma|E_+|^2E_+=0,$$

$$-i\frac{\partial E_-}{\partial x}+\frac{i}{v_g}\frac{\partial E_-}{\partial t}+\kappa(x)E_++\delta(x)E_-+2\Gamma|E_+|^2E_-+\Gamma|E_-|^2E_-=0, \tag{4}$$

where [17–19]

$$\kappa(x)=\frac{\pi\Delta n(x)}{\lambda},$$

$$\delta(x)=\frac{2\pi\delta n(x)}{\lambda}-\frac{1}{2}\frac{d\vartheta}{dx},$$

$$\Gamma=\frac{4\pi n_0}{\lambda Z}n^{(2)} \tag{5}$$

are all real. Further, v_g is the group velocity at ω_0 in the absence of a grating, λ is the free space wavelength, and Z the vacuum impedance. The parameter $\kappa(x)$ gives the strength of the grating, while $\delta(x)$ describes the detuning of the Bragg frequency from ω_0. Nonlinear effects are described by Γ, which we take to be constant in space, although this is not essential.

Though ultimately we are interested in gratings for which both κ and δ are periodic, and $\Gamma\neq0$, we now briefly consider uniform linear gratings for which κ and δ are constant and $\Gamma=0$, as some of the concepts carry over. Under the conditions discussed above, we first consider the uniform grating's dispersion relation [14,19]. Substituting

$$E_\pm(x,t)=A_\pm e^{i(kx-v_g\Delta t)}, \tag{6}$$

where the detuning Δ is related to the actual frequency ω through

$$\Delta=\frac{\omega-\omega_0}{v_g}, \tag{7}$$

we find that Eqs. (4) lead to two coupled linear algebraic equations. Nontrivial solutions can be found when

$$\Delta=-\delta+\sqrt{\kappa^2+k^2}. \tag{8}$$

This relation is indicated by long-dashed lines in Fig. 2; subscripts on the symbols should for now be ignored. Figure 2 shows that for $-\delta-\kappa<\Delta<-\delta+\kappa$ no plane-wave solutions exist; this corresponds to the photonic band gap of the uniform grating. The center of the photonic band gap, at $\Delta=-\delta$, corresponds to the Bragg frequency.

A. Linear properties of SSG

As mentioned in Sec. I, our procedure for deep SSG's requires knowledge of the Bloch functions of these structures. To define these we write the *linear* coupled mode equations as [13]

$$\frac{i}{v_g}\frac{\partial\mathbf{E}}{\partial t}=\mathbf{M}(x)\mathbf{E}, \tag{9}$$

where $\mathbf{E}$ is the vector with elements (E_+,E_-), and $\mathbf{M}$ is the operator defined as

$$\mathbf{M}(x)=\begin{pmatrix}-i\partial/\partial x-\delta(x) & -\kappa(x)\\ -\kappa(x) & +i\partial/\partial x-\delta(x)\end{pmatrix}. \tag{10}$$

For SSG's, the key property of $\mathbf{M}$ is that it is periodic with period Λ, so that

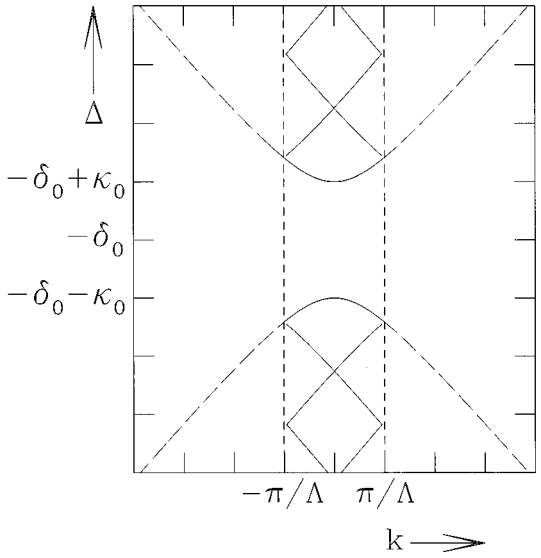

FIG. 2. The dispersion relation for a uniform grating, given by Eq. (16), is indicated by the dashed line. The introduction of an infinitesimally weak periodicity with period Λ causes the dispersion relation to fold in the first Brillouin zone between $\pm\pi/\Lambda$ (solid line).

$$\mathbf{M}(x+\Lambda)=\mathbf{M}(x). \tag{11}$$

We now search for the eigenvectors Ψ, with elements (ψ_+,ψ_-) of $\mathbf{M}$, by setting [13]

$$\mathbf{E}=\mathbf{\Psi}e^{-iv_g\Delta t}, \tag{12}$$

so that

$$\mathbf{M}\Psi=\Delta\Psi; \tag{13}$$

because of the periodicity of $\mathbf{M}$ we refer to the Ψ as the *Bloch functions* [14].

We have now recast the coupled mode equations into a Schrödinger-equation-like formalism, with $\mathbf{M}$ playing the role of the Hamiltonian. Indeed many of the results from quantum mechanics concerning periodic potentials can be applied to SSG's with little modifications. The most important of these is Bloch's theorem according to which the solutions to Eq. (13) with $\mathbf{M}$ satisfying Eq. (11) must have the property [20,21]

$$\Psi(x+\Lambda)=e^{ik\Lambda}\Psi(x), \tag{14}$$

for some real number k. This restatement of Bloch's theorem can be proven by a straightforward adaption of, for example, the approach in Ziman [20]. Equation (14) implies that an eigenfunction of $\mathbf{M}$ can be written as

$$\Psi(x)=\begin{pmatrix}h_+(x)\\ h_-(x)\end{pmatrix}e^{ikx} \tag{15}$$

with the associated eigenvalue Δ. As in solid-state physics [21,20], the functions $h_\pm$ are periodic with period Λ. The real number k is the reduced wave number, which is usually chosen in the first Brillouin zone, where $-\pi/\Lambda<k\leqslant+\pi/\Lambda$; it labels the eigenvalues and eigenfunctions of $\mathbf{M}$. For a periodic system it is expected that for fixed k, the eigenvalues of $\mathbf{M}$ are discrete, as is true in quantum mechanics [20,21]. This implies that the allowed detunings Δ, corresponding to the eigenvalues of $\mathbf{M}$, can be labeled by integers. Thus for a SSG each Bloch function has two ''quantum numbers'': an integer n which labels the band, and the (real) reduced wave number k. Usually one considers the eigenvalues Δ_{nk} to be functions of k, which immediately leads to the photonic band structure: the photonic band diagram for a SSG is obtained by plotting the Δ_{nk} versus k. We illustrate these general statements in Sec. II B.

B. Photonic band structure of SSG's

Before illustrating the discussion in Sec. II A with a complete photonic band diagram, we first treat the limiting case where the SSG is a small perturbation to a uniform grating. This allows us to find the approximate positions of the Rowland ghost gaps in the dispersion relation analytically. For a general SSG, let κ_0 and δ_0 be the zeroth-order Fourier components of $\kappa(x)$ and $\delta(x)$. The SSG is then considered a perturbation, characterized by the other Fourier coefficients, to a uniform grating with strength κ_0 and center frequency $\Delta=-\delta_0$. The dispersion relationship for the uniform grating is [Eq. (8)]

$$\Delta=-\delta_0\pm\sqrt{k^2+\kappa_0^2}, \tag{16}$$

where the wave number k can take on any value (long-dashed lines in Fig. 2). Introducing an infinitesimally weak periodic perturbation with period Λ, we now apply the standard results from condensed matter physics (see the last paragraph of Sec. II A): k represents a reduced wave number within the first Brillouin zone: $-\pi/\Lambda<k\leqslant+\pi/\Lambda$ [20,21]. As mentioned, this restriction of k implies that Δ is now a multivalued function of k, as illustrated by the solid lines in Fig. 2.

Folding the uniform grating dispersion relation into the first Brillouin zone causes crossings of the dispersion relation at the edges and in the center of the Brillouin zone at detunings

$$D_\ell=-\delta_0+\mathrm{sgn}(\ell)\sqrt{\left(\frac{\ell\pi}{\Lambda}\right)^2+\kappa_0^2},\quad \ell\in\mathbb{Z} \tag{17}$$

with the exception of $\ell=0$ (see Fig. 2). The function sgn (ℓ) is defined by $\mathrm{sgn}(\ell)=1$ if $\ell>0$, $\mathrm{sgn}(0)=0$ and $\mathrm{sgn}(\ell)=-1$ if $\ell<0$. It is at these detunings that gaps open up due to Bragg reflection as the strength of the SSG increases.

For weak SSG's previous authors have stated [8] that the width of the gap centered around D_n is $2|\kappa_n|$, where κ_n is the strength of the nth Fourier coefficient of κ; we confirm this in the Appendix, though we also prove somewhat more general results valid under less restricitve conditions. But for a deep SSG these predictions break down and a different formalism must be used. Nevertheless the gaps occur at detunings given by Eq. (17), when $k=0$ or $k=\pi/\Lambda$. The opening of gaps in the dispersion relation can be seen in Fig. 3(a), which shows the full dispersion relation of the SSG in Fig. 1. We took ϑ in Eq. (1) a constant, and $\delta n=\Delta n$, as is usually

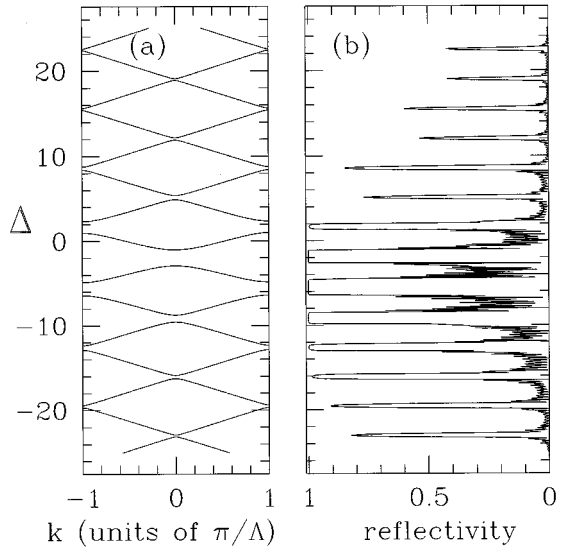

FIG. 3. (a) Band diagram for the triangular SSG discussed in the text and shown in Fig. 1. The Rowland ghost gaps are centered on the detunings $D_2 \approx 5\ \mathrm{cm}^{-1}$, $D_1 \approx 1.5\ \mathrm{cm}^{-1}$, $D_0 \approx -2\ \mathrm{cm}^{-1}$, $D_{-1} \approx -5.5\ \mathrm{cm}^{-1}$, $D_{-2} \approx -9\ \mathrm{cm}^{-1}$, etc., given by Eq. (17). The corresponding reflection spectrum is shown in (b); note that the Rowland ghost gaps correspond to detunings with high reflectivity.

the case in optical fibers [17], so that, with Eqs. (5), $\delta = 2\kappa$. In Fig. 3(a) $D_2 \approx 5\ \mathrm{cm}^{-1}$, $D_1 \approx 1.5\ \mathrm{cm}^{-1}$, $D_0 \approx -2\ \mathrm{cm}^{-1}$, $D_{-1} \approx -5.5\ \mathrm{cm}^{-1}$, $D_{-2} \approx -9\ \mathrm{cm}^{-1}$, etc., consistent with Eq. (17).

For most SSG's analytic solutions to Eq. (13) are not known and the Bloch functions and dispersion relation must be found numerically. A method to do this is described in the Appendix [21]; the bands in Fig. 3(a) were obtained using this method. In Fig. 3(b) we show the associated reflection spectrum. Clearly each peak in the reflection spectrum corresponds to a gap in the dispersion relation for the SSG. Following the notation used to describe periodic errors in diffraction gratings [7] we refer to the reflection peaks as Rowland ghosts, and to the corresponding gap in the dispersion relation as Rowland ghost gaps. We note that the standard Fourier treatment of shallow SSG's (see Sec. I) requires that the reflection peaks of the SSG are sufficiently spaced to be able to treat them as independent. Though this is a good approximation for the reflection peaks with $\Delta > 5$ and $\Delta < -10$ in Fig. 3(b), it is clearly suspicious for the strong central reflection peaks, for which the spacing roughly equals the width.

We can now formulate a rough criterion for a superstructure to be deep. The centers of two adjacent gaps at the edge or the center of the Brillouin zone are spaced by a frequency, approximately given by [see Eq. (20)]

$$\frac{\pi}{\Lambda} v_g . \tag{18}$$

As shown in the Appendix below Eq. (A12), in a shallow grating the width of a gap is of order [8]

$$2 v_g |\kappa_n|, \tag{19}$$

where κ_n is the strength of the nth Fourier component of κ. For the various reflection peaks to be independent, we require the associated gaps not to be too close. We thus find that for a superstructure to be shallow, it is necessary that

$$|\kappa_n| \Lambda \ll \frac{\pi}{2} \approx 1, \tag{20}$$

for all appropriate Fourier components. If at least one of these inequalities is not satisfied, then the grating cannot be treated as shallow over its entire spectrum. At this point we note that there is some ambiguity as to how one would define a shallow SSG. The implicit choice in the literature [3,8] corresponds to applying inequality (20) to *all* Fourier components of the SSG. However, in the Appendix we argue that the inclusion in (20) of $n = 0$, the Fourier component associated with the underlying uniform grating, can lead to paradoxical results. We return to this in Sec. A 1. From Fig. 1 we estimate the left-hand side of Eq. (20) to be about 0.7 for $n = \pm 1$, confirming that, by either criterion, the SSG is not shallow at all detunings.

C. Properties of Bloch functions

Before continuing we need to establish some key properties of Bloch functions. From Eq. (10) it can be seen that if Ψ with components $[\psi_+(x), \psi_-(x)]$ is an eigenfunction of $\mathbf{M}$, then for any real number ξ so is

$$\overline{\Psi} \equiv e^{i\xi} \begin{pmatrix} \psi_-^* \\ \psi_+^* \end{pmatrix} \tag{21}$$

with the same eigenvalue Δ as Ψ. Furthermore Bloch's theorem implies that if Ψ has a reduced wave number k, then $\overline{\Psi}$ has the reduced wave number $-k$. Physically the solution $\overline{\Psi}$ corresponds to the same solution as Ψ but moving with the opposite group velocity. This implies that the photonic band diagram must have inversion symmetry about $k = 0$, as is seen in Fig. 3(b).

However, since gaps occur at $k = 0, \pm \pi/d$, if Ψ is a Bloch function at the top or bottom of a gap, then so is $\overline{\Psi}$ defined by Eq. (21), and furthermore it is associated with the same point of the dispersion relation as Ψ. Since for a particular k and Δ the (normalized) Bloch functions are unique up to a constant phase, we must then have

$$\overline{\Psi} = \Psi \tag{22}$$

for some phase angle ξ in Eq. (21). If we make the transformation $\Psi \rightarrow \exp(-i\xi/2)\Psi$, then Eq. (22) implies that

$$\mathbf{\Psi} = \begin{pmatrix} \psi(x) \\ \psi(x)^* \end{pmatrix}. \tag{23}$$

We now choose the phases of ψ_+ and ψ_- such that at the edges of any Rowland ghost gap Eq. (23) is satisfied.

Figure 4 shows the moduli of the Bloch functions at the top (solid line) and bottom (dashed line) of the Rowland ghost gap centered on $D_1 \approx 1.5\ \mathrm{cm}^{-1}$. By comparing Fig. 1 of the grating profile and Fig. 4 we see that at positions

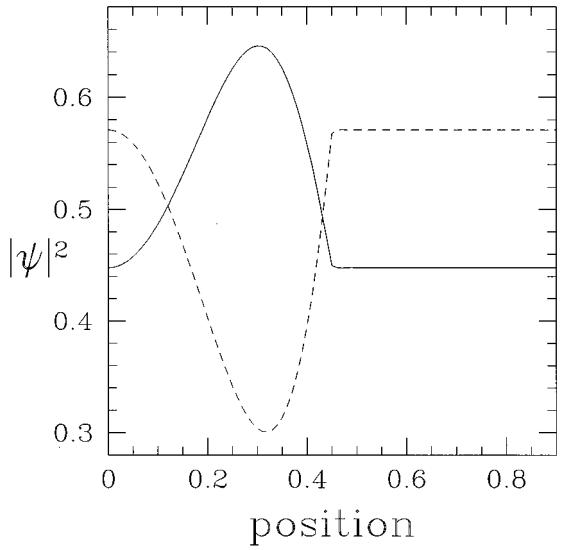

FIG. 4. Bloch functions at the top and bottom of the gap centered around $\Delta \approx 1.5$ at the edge of the Brillouin zone. The solid line is $|\psi_+(x)|^2 = |\psi_-(x)|^2$ at the top of the gap, while the dashed line gives that at the bottom. Recall that according to the discussion in Sec. II C the square moduli of the two components of a Bloch function are the same.

where the grating strength vanishes the Bloch functions have a constant intensity. This is as expected, as in these regions light freely propagates.

D. Preliminary results

Here we establish some preliminary results which will prove useful when deriving the supercoupled mode equations. Eigenvalue equation (13) is equivalent to Eq. (9) from Ref. [13]. Much of the derivations following this equation can be carried over straightforwardly to the present case. In particular, we adopt the normalization

$$\int_0^L dx \Psi^\dagger \cdot \Psi = N, \tag{24}$$

where L is the normalization length over which the periodic boundary conditions are applied, and $N \equiv L/\Lambda$ is the number of periods in L. A feature of normalization (24) is the absence of a nonconstant metric or kernel; this should be contrasted to related systems where the refractive index [13] or the dielectric function [22] play this role. Apart from the sign then, convention (23) and normalization (24) uniquely specify the Bloch functions at the edges of each Rowland ghost gap.

Using a $\mathbf{k}\cdot\mathbf{V}$ expansion as in Ref. [13], it can be proven that the group velocity Δ'_{mk} and the group velocity dispersion Δ''_{mk} associated with a position on the dispersion relation indicated by k and n are given by

$$\Delta'_{nk} = \frac{\partial \Delta_{nk}}{\partial k} = v_{nn}(k),$$

$$\Delta''_{nk} = \frac{\partial^2 \Delta_{nk}}{\partial k^2} = -2 \sum_{p \neq n} \frac{v_{pn}(k) v_{np}(k)}{\Delta_{pk} - \Delta_{nk}}, \tag{25}$$

where

$$v_{pn}(k) = \frac{1}{N} \int_0^L dx \Psi_{pk}^\dagger \sigma_z \Psi_{nk} = \frac{1}{N} \int_0^L dx \mathbf{h}_{pk}^\dagger \sigma_z \mathbf{h}_{nk}, \tag{26}$$

where $\mathbf{h}$ is the column vector with the elements (h_+, h_-) [see Eq. (15)] and σ_z is the Pauli matrix diag$(1,-1)$. At the edges and in the center of the Brilouin zone the group velocity vanishes [see Fig. 3(a)], so that the first of Eqs. (25) with Eq. (26) implies that $|\psi_+|^2 = |\psi_-|^2$, confirming that the net energy transport vanishes.

III. EVOLUTION EQUATIONS FOR SUPERENVELOPES

Here we present the derivation of the supercoupled mode equations which describe light propagation through a nonlinear SSG. Briefly, this approach can be understood as follows. It is well known that applying standard coupled mode theory to a uniform grating allows one to replace the Maxwell equations with *periodic* coefficients, with coupled mode equations with *constant* coefficients. Such an approach is valid for a range of frequencies about one of the Bragg frequencies of the periodic structure. For SSG's, which are characterized by a doubly periodic refractive index [see Eq. (1)], applying standard coupled mode theory then allows us to replace Maxwell's equations by the coupled mode equations with periodic coefficients [Eqs. (4)]. Presumably, then, applying a coupled-mode-like theory to the latter would be expected to result in a set of equations (supercoupled mode equations) with constant coefficients. Such a supercoupled mode theory would be valid close to one of the Rowland ghost gaps shown in Fig. 3(a). Below we show this to be true.

Below we take two approaches to deriving evolution equations for the superenvelopes. First we expand the envelopes in terms of a single Bloch function of the field envelopes (Sec. III A) which leads to the nonlinear Schrödinger equation. In Sec. III B we expand in terms of two such Bloch functions, leading to the supercoupled mode equations (Sec. III C).

A. Single-band approximation: The nonlinear Schrödinger equation

Here we take the envelopes $\mathbf{E}$ of the form

$$\mathbf{E}(x,t) = a(x,t) \Psi_{nk}(x) e^{-i v_g \Delta_{nk} t}, \tag{27}$$

where $\Psi_{nk}(x)$ is a Bloch function of the superstructure, while Δ_{nk} indicates its eigendetuning. Here $\Psi_{nk}(x)$ is taken to be at the edge of one of the Rowland ghost gaps (such as those in Fig. 3), though this is not essential. In Eq. (27), $a(x,t)$ is a function which varies slowly compared to the Bloch function of the superstructure; we thus require that a varies slowly compared to Λ. By the same argument we also require a to vary slowly in time on the scale of $(v_g \kappa_0)^{-1}$. Since $a(x,t)$ varies slowly in space and time on the scale of the usual envelope functions of the electric field we refer to it as a superenvelope.

We now substitute ansatz (27) for the field into the coupled mode equations and find the evolution equation for the superenvelope $a(x,t)$. As mentioned, the details of this procedure are virtually identical to those described in Sec.

V B of Ref. [13] and so we do not repeat them here. The only difference is that the envelopes $E_{\pm}$ are complex, while the actual electric and magnetic fields are, of course, real. We therefore do not need to take the real part of Eq. (27) as was done in the corresponding Eq. (68) in Ref. [13]. Following now Ref. [13] we find that $a(x,t)$ satisfies a nonlinear Schrödinger equation,

$$i\left(\frac{\partial a}{\partial t}+\Delta'_{nk}\frac{\partial a}{\partial x}\right)+\frac{1}{2}\Delta''_{nk}\frac{\partial^2 a}{\partial z^2}+\alpha|a|^2a=0. \tag{28}$$

Here Δ'_{nk} is the group velocity associated with Ψ_{nk}, while Δ''_{nk} is its group velocity dispersion [Eqs. (25)]. Finally, α is an effective nonlinearity, which is given in terms of a nonlinear overlap of Ψ_{nk}:

$$\alpha=\Gamma\int_0^L dx\ (|\psi_+|^4+4|\psi_+\psi_-|^2+|\psi_-|^4\ )=6\Gamma\int_0^L dx|\psi_+|^2, \tag{29}$$

where the $\psi_{\pm}$ are the components of Ψ_{nk}, and for the last equality we have used Eq. (23), so that it is only valid at $k=0$ and $k=\pm\pi/\Lambda$. The nonlinear Schrödinger equation is well known to have soliton solutions. The significance of these solutions in the context of SSG's is discussed in the sections below.

The accuracy of one-band approximations, where k was taken to be at the edge of a photonic band gap, was studied before [22]. It was found that it is valid only over the narrow range of frequencies for which mixing of Bloch functions can be ignored [22]. It is likely that the one-band approach is better when Ψ_{nk} is taken to be away from any of the gaps, but since grating effects are then not very prominent this is not of primary interest.

Using the explicit expressions for the Bloch functions in the center and at the edges of the Brillouin zone in the shallow SSG limit [Eqs. (A14) and (A16)] it is easily found that in this limit

$$\Delta'=0,$$

$$\Delta''=\pm\frac{\cos\varphi_{\diagup}}{\kappa_{\diagup}},$$

$$\alpha=\frac{3\Gamma}{4\Lambda}(2+\sin^2\varphi_{\diagup})N, \tag{30}$$

where the $\varphi_{\diagup}$ are defined in Eqs. (A12). Because the group velocity always vanishes for $k=0,\pi/d$, the first of these is true for any SSG. Further, through N, α depends explicitly on the normalization length L. This can easily be avoided by defining $\overline{a(x,t)}=a\sqrt{N}$ [22], for which the nonlinear parameter does not depend on N at all.

B. Two-band approximation

A more general approach than Eq. (27) involves two Bloch functions and two superenvelopes,

$$\mathbf{E}(x,t)=[f_u(x,t)\Psi_u(x)+f_l(x,t)\Psi_l(x)]e^{-iv_g\Delta_0 t}, \tag{31}$$

which is the approach we concentrate on henceforth. We take the $\Psi_{u,l}$ to be Bloch functions at the upper and lower edges of one of the Rowland ghost gaps [Fig. 3(a)], respectively, as this describes the situation of most interest. Writing the eigendetunings as $\Delta_{u,l}$, we define

$$\Delta_0=\frac{1}{2}(\Delta_u+\Delta_l), \tag{32}$$

corresponding to the center of the Rowland ghost gap under consideration. Finally, the $f_{u,l}(x,t)$ in Eq. (31) are slowly varying superenvelope functions. Ansatz (31) is similar to Eq. (80) in Ref. [13], and the analysis in Sec. VI B straightforwardly carries over to SSG's; again, the only difference is that the $E_{\pm}$ are complex functions, while the electric and magnetic fields are real.

Following then the derivation of de Sterke *et al.* [13], the superenvelopes $f_{u,l}$ can be shown to satisfy a set of *supercoupled mode equations* of the form

$$\begin{aligned}
i\frac{\partial f_u}{\partial t}&=\sigma f_u+V\frac{\partial f_l}{\partial x}-\alpha_1|f_u|^2f_u-\alpha_2|f_l|^2f_l\\
&\quad-\alpha_3(2|f_u|^2f_l+f_u^2f_l^*)-\alpha_4(2|f_l|^2f_u+f_l^2f_u^*),\\
i\frac{\partial f_l}{\partial t}&=-\sigma f_l-V\frac{\partial f_u}{\partial x}-\alpha_3|f_u|^2f_u-\alpha_5|f_l|^2f_l\\
&\quad-\alpha_4(2|f_u|^2f_l+f_u^2f_l^*)-\alpha_2(2|f_l|^2f_u+f_l^2f_u^*).
\end{aligned} \tag{33}$$

Here,

$$\sigma=\Delta_u-\Delta_0=\Delta_0-\Delta_l, \tag{34}$$

where the last equality follows from Eq. (32), and

$$V=iv_{ul} \tag{35}$$

is real, as can be ascertained from definition (26) and convention (23). Finally, the α are various nonlinear overlap integrals of the Bloch functions, defined as

$$\alpha_1=6\Gamma\int_0^L dx|\psi_{+u}|^4,$$

$$\alpha_2=3\Gamma\int_0^L dx|\psi_{+l}|^2(\psi_{+l}\psi_{+u}^*+\psi_{+l}^*\psi_{+u}),$$

$$\alpha_3=3\Gamma\int_0^L dx|\psi_{+u}|^2(\psi_{+l}\psi_{+u}^*+\psi_{+l}^*\psi_{+u}),$$

$$\alpha_4=\Gamma\int_0^L dx\{4|\psi_{+u}\psi_{+l}|^2+[(\psi_{+l}\psi_{+u}^*)^2+(\psi_{+l}^*\psi_{+u})^2]\},$$

$$\alpha_5=6\Gamma\int_0^L dx|\psi_{+l}|^4, \tag{36}$$

where $\psi_{+u,l}$ is the first element of $\Psi_{u,l}$. Note that it follows immediately from the definitions that all α_i are real. In ad-

dition, using the method described in Ref. [23] we can find inequalities pertaining to the magnitudes of the α_i. First note that by inspection

$$\alpha_4 \leqslant \overline{\alpha_4} \equiv 6 \int_0^L dx |\psi_{+u}\psi_{+l}|^2. \tag{37}$$

Then, using the method in Ref. [23] it is straightforward to prove the Schwarz inequality

$$\alpha_1\alpha_5 \geqslant \overline{\alpha_4^2} \geqslant \alpha_4^2. \tag{38}$$

Another inequality can be formulated if one first defines

$$\alpha_2 \leqslant \overline{\alpha_2} \equiv 6 \int_0^L dx |\psi_{+u}\psi_{+l}^3|,$$

$$\alpha_3 \leqslant \overline{\alpha_3} \equiv 6 \int_0^L dx |\psi_{+l}\psi_{+u}^3|. \tag{39}$$

Then write the argument of the right-hand side of the first inequality (39) as $|\psi_{+l}|^2 \times |\psi_{+u}\psi_{+l}|$, and that of the second as $|\psi_{+u}|^2 \times |\psi_{+u}\psi_{+l}|$. Applying the Schwarz inequality to each of these, it can then be shown that

$$\alpha_1\alpha_5 \geqslant \overline{\alpha_2}\,\overline{\alpha_3} \geqslant \alpha_2\alpha_3. \tag{40}$$

Equations (33) are identical to Eqs. (100) in Ref. [13]. However, in the subsequent step in this reference only the special case $k=0,\pi/d$, where $\alpha_2=\alpha_3=0$, is considered. Note that in the present case of SSG's, we also restrict ourselves to the center and edges of the Brillouin zone, but now α_2, α_3 generally do not vanish.

C. Transformation to supercoupled mode equations

Equations (33) take on a more familiar form if we introduce the superenvelopes $f_\pm$ through [13,24]

$$f_\pm = f_l \mp i f_u. \tag{41}$$

In terms of these new envelope functions the supercoupled mode equations (SCME's) attain their final form:

$$\begin{aligned} i\frac{\partial f_+}{\partial x} + \frac{i}{V}\frac{\partial f_+}{\partial t} + \widetilde{\kappa} f_- + \widetilde{\Gamma}|f_+|^2 f_+ + 2\widetilde{\Gamma}|f_-|^2 f_+ + \Gamma_1(|f_+|^2 \\ + |f_-|^2) f_- + (\Gamma_1 f_- f_+^* + \Gamma_1^* f_+ f_-^*) f_+ + \Gamma_2 f_-^2 f_+^* = 0, \\ i\frac{\partial f_-}{\partial x} + \frac{i}{V}\frac{\partial f_-}{\partial t} + \widetilde{\kappa} f_+ + \widetilde{\Gamma}|f_-|^2 f_- + 2\widetilde{\Gamma}|f_+|^2 f_- + \Gamma_1^*(|f_+|^2 \\ + |f_-|^2) f_+ + (\Gamma_1 f_- f_+^* + \Gamma_1^* f_+ f_-^*) f_- + \Gamma_2^* f_+^2 f_-^* = 0. \end{aligned} \tag{42}$$

Here

$$\widetilde{\kappa} = \frac{\sigma}{V}, \tag{43}$$

and the nonlinear coefficients are linear combinations of the α_i [Eqs. (36)], given by

$$\begin{aligned} \widetilde{\Gamma} &= \frac{1}{8V}(\alpha_1 + 2\alpha_4 + \alpha_5), \\ \Gamma_1 &= \frac{1}{8V}[(-\alpha_1 + \alpha_5) - 2i(\alpha_2 + \alpha_3)], \\ \Gamma_2 &= \frac{1}{8V}[(\alpha_1 - 6\alpha_4 + \alpha_5) - 4i(\alpha_2 - \alpha_3)]. \end{aligned} \tag{44}$$

Thus $\widetilde{\Gamma}$ is real, while $\Gamma_{1,2}$ generally are complex. As mentioned, Eqs. (42) are identical to the coupled mode equation for deep gratings, except that in the latter case, for $k=0,\pi/d$, $\alpha_2=\alpha_3=0$, so that all nonlinear coefficients are real. We note that despite $\Gamma_{1,2}$ being complex in Eqs. (42), we find that

$$\frac{\partial}{\partial t}(|f_+|^2 + |f_-|^2) = \frac{\partial}{\partial x}(|f_+|^2 - |f_-|^2), \tag{45}$$

indicating that energy is conserved, as required for a lossless system.

Using inequality (38) it is easy to show that

$$|\Gamma_{1r}|, |\Gamma_{2r}| \leqslant \widetilde{\Gamma}, \tag{46}$$

where Γ_{jr} indicates the real part of Γ_j. Also, using inequality (40) we can formulate an inequality in terms of the imaginary parts of $\Gamma_{1,2}$; however, it appears not to be very useful, and we do not give it here.

We now first consider the shallow SSG limit of the results derived above. By substituting expressions (A14) and (A16) for the Bloch functions of a shallow SSG into definitions (36) it is found that

$$\alpha_2 = \alpha_3 = 0, \quad \alpha_1 = \alpha_5 = 3\alpha_4, \tag{47}$$

consistent with inequality (38). Thus we find from Eqs. (44) that $\Gamma_{1,2}=0$. The SCME's for a shallow SSG thus have the same form as the coupled mode equations for a *shallow uniform grating* [2] [i.e., Eqs. (4) with constant coefficients [18,19]]. We comment on this below. Using Eqs. (A14) and (A16) it is found that in the shallow SSG limit

$$\widetilde{\Gamma} = \frac{N\Gamma}{4\Lambda v_g}(2 + \sin^2\varphi_{\ell}). \tag{48}$$

Thus just like coefficient α in the nonlinear Schrödinger equation [Eq. (30)], $\widetilde{\Gamma}$ depends on the normalization length, via N; it is removed by considering the evolution of the superenvelopes $f_\pm\sqrt{N}$ [22].

Another case for which the general SCME's simplify is when the SSG is an even function of position. This implies that all the Fourier coefficients can be made real. Then matrix A [Eqs. (A8) and (A10)] is real and symmetric, and it thus has real eigenvectors. It can be shown that now the first set of Eqs. (47) still holds, but that the second does not. Thus, from Eqs. (44), all Γ's are real, but $\Gamma_{1,2} \neq 0$. The SCME are now identical to the coupled mode equations for deep gratings [13]; solutions to these equations have been discussed by de Sterke *et al.* [13].

We finally note that numerical examination of a wide variety of SSG's suggests that the moduli of the new nonlinear coefficients Γ_1 and Γ_2 tend to be smaller than $\tilde{\Gamma}$. If we neglect these coefficients, the SCMEs are formally identical to the nonlinear coupled mode equations (4) with constant coefficients [16]. Thus, for frequencies sufficiently close to a Rowland ghost gap, a nonlinear SSG then behaves identically to a shallow uniform nonlinear grating; we showed above that this is also generally true for shallow SSG's. Since previously a variety of solitary wave solutions for shallow gratings have been found, these immediately carry over to a large class of SSG's. These solutions include bright solitary wave solutions, referred to as *gap solitons* or *grating solitons* in the context of uniform gratings [19,26–28], and *Rowland ghost solitons* in the context of SSG's [5,16]; dark solutions and bright solutions on a pedestal are also known [13,29]. Rowland ghost solitons represent high-intensity pulses propagating through the SSG without changing shape, at velocities which can be substantially below that in bare fiber. This has been verified numerically by Broderick *et al.* [16], and experimentally, in an optical fiber geometry, by Eggleton *et al.* [5].

In Sec. IV we discuss bright solitary wave solutions to the SCME for the general case in which the simplifications listed above do not apply.

IV. SOLITARY WAVES IN ROWLAND GHOST GAPS

In Sec. III we showed that for frequencies close to a ghost gap the original coupled mode equations (4) with periodic coefficients can be approximated by the supercoupled mode equations (42) with constant coefficients. In this section we focus on soliton solutions to the most general version of these equations in which the $\Gamma_{1,2}$ are complex.

For gratings for which the new nonlinear coefficients $\Gamma_{1,2}$ are complex and are comparable in magnitude to $\tilde{\Gamma}$, we can find stationary soliton solutions using a method earlier used by Kivshar and Flytzanis [25] and de Sterke *et al.* [13]. To use this method we start from Eqs. (33), which of course are equivalent to the SCME (42). Introducing the superenvelopes $u_{1,2}$ through

$$f_l = u_1 e^{-i\tilde{\Delta}t}, \quad f_u = u_2 e^{-i\tilde{\Delta}t}, \tag{49}$$

and taking $u_{1,2}$ to be *real*, we find

$$\begin{aligned} u_1' &= -\tilde{\Delta}_2 u_2 + \alpha_1 u_2^3 + \alpha_2 u_1^3 + 3\alpha_3 u_1 u_2^2 + 3\alpha_4 u_1^2 u_2, \\ u_2' &= +\tilde{\Delta}_1 u_1 - \alpha_3 u_2^3 - \alpha_5 u_1^3 - 3\alpha_4 u_1 u_2^2 - 3\alpha_2 u_1^2 u_2, \end{aligned} \tag{50}$$

where the prime indicates differentiation with respect to x/V, and

$$\tilde{\Delta}_1 = -\sigma - \tilde{\Delta}, \quad \tilde{\Delta}_2 = \sigma - \tilde{\Delta}. \tag{51}$$

These equations can be derived from the Hamiltonian [25,13]

$$\begin{aligned} \mathcal{H} = &-\frac{1}{2}(\tilde{\Delta}_1 u_1^2 + \tilde{\Delta}_2 u_2^2) \\ &+ \frac{1}{4}(\alpha_1 u_2^4 + 4\alpha_3 u_1 u_2^3 + 6\alpha_4 u_1^2 u_2^2 + 4\alpha_2 u_1^3 u_2 + \alpha_5 u_1^4). \end{aligned} \tag{52}$$

It is well known [13,25] that the separatrices of system (50) correspond to stationary solitary wave solutions to the SCME [Eq. (42)]. Thus to give a complete analysis of such solutions we would require a classification of all critical points of Eq. (50). However, here we limit ourselves to frequencies within the photonic band gap for which $-\sigma < \tilde{\Delta} < +\sigma$, so that, from Eqs. (51), $\Delta_1 < 0$, $\Delta_2 > 0$. Equations (50) show that the origin is now a saddle point [13,25]; the associated separatrix can be found via the evolution equation for the ratio $r \equiv u_1/u_2$ [25]:

$$\begin{aligned} (r')^2 = &(\tilde{\Delta}_2 + \tilde{\Delta}_1 r^2) \\ &+ 4E(\alpha_1 + 4\alpha_3 r + 6\alpha_4 r^2 + 4\alpha_2 r^3 + \alpha_5 r^4), \end{aligned} \tag{53}$$

where E is the ''energy'' associated with Hamiltonian $\mathcal{H}$. Concentrating on the separatrix starting and finishing at the origin, we take $E = 0$, and find [25,13]

$$r = \sqrt{\frac{-\tilde{\Delta}_2}{\tilde{\Delta}_1}}\tanh(\sqrt{-\tilde{\Delta}_1\tilde{\Delta}_2}\,x/V) \equiv \sqrt{\frac{-\tilde{\Delta}_2}{\tilde{\Delta}_1}}\tanh(Cx). \tag{54}$$

Using this result it is straightforward to show that system (50) has the solution

$$\begin{aligned} u_1 &= \sqrt{\frac{-2\tilde{\Delta}_1\tilde{\Delta}_2^2}{B}}\sinh(Cx), \\ u_2 &= \sqrt{\frac{2\tilde{\Delta}_1^2\tilde{\Delta}_2}{B}}\cosh(Cx), \end{aligned} \tag{55}$$

where the denominator B is given by

$$\begin{aligned} B = &\alpha_1\tilde{\Delta}_1^2 c^4 + 4\alpha_3(-\tilde{\Delta}_1^3\tilde{\Delta}_2)^{1/2} c^3 s + 6\alpha_4(-\tilde{\Delta}_1\tilde{\Delta}_2)c^2 s^2 \\ &+ 4\alpha_2(-\tilde{\Delta}_1\tilde{\Delta}_2^3)^{1/2} c s^3 + \alpha_5\tilde{\Delta}_2^2 s^4, \end{aligned} \tag{56}$$

where

$$c = \cosh(Cx), \quad s = \sinh(Cx), \tag{57}$$

and the constant C was defined in Eq. (54).

From transformation (41) it can be seen that Eqs. (55) represent a solution to Eqs. (42) with $f_- = f_+^*$ consistent with the properties of the stationary solutions of similar systems [13,19,25]. However, an important difference is that the solutions represented by Eqs. (55) are *asymmetric*, due to the presence of the α_2 and α_3 terms. This is illustrated in Figs. 5 and 6. Figure 5 shows the separatrix in the u_1, u_2 plane for the parameters

$$V = 1, \quad \tilde{\kappa} = 1, \quad \tilde{\Delta} = -0.5, \quad \alpha_1 = 1.7,$$

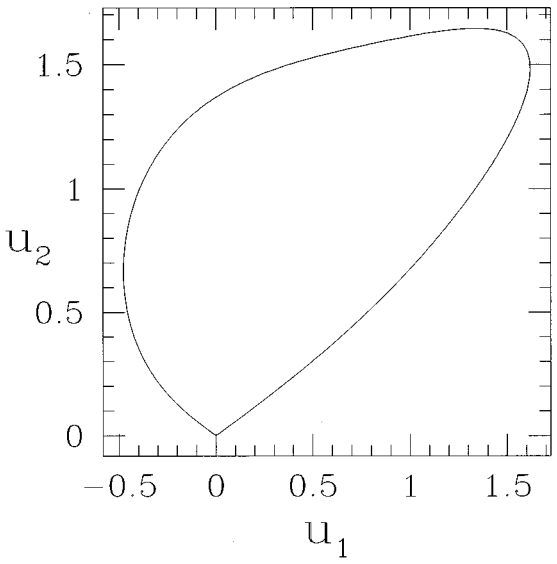

FIG. 5. Separatrix of dynamical system (50) for parameters given in Eq. (58) given by Eq. (55). Since Γ_1 and Γ_2 are complex, this implies, via Eqs. (44), that α_2 and α_3 are nonzero, leading to the asymmetry of the separatrix.

$$\alpha_2=-0.7, \quad \alpha_3=-0.5, \quad \alpha_4=0.3, \quad \alpha_5=1.7; \quad (58)$$

it exhibits no symmetry, in contrast to the corresponding curves for uniform gratings [13]. The associated solution to the SCME's is given in Fig. 6, which shows $u_1^2+u_2^2=|f_\pm|^2$ as a function of position; it is also asymmetric. As an aside we mention that Hamiltonian (52) always has inversion symmetry with respect to the origin; this implies the existence of a separatrix like that shown in Fig. 5, but inverted. However, the field densities associated with these solutions are the same as those in Fig. 6.

Equations (55) represent stationary bright solitary wave solutions to Eqs. (33), and thus, via transformation (41), to Eqs. (42) as well; they are a generalization of previously found solutions for deep [13] and shallow gratings [27].

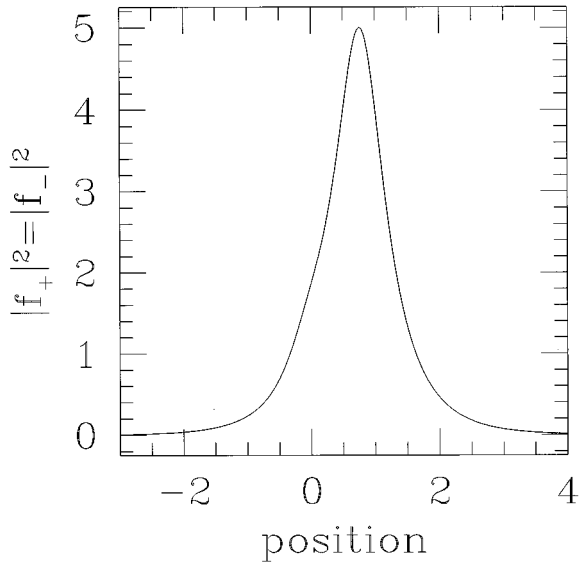

FIG. 6. Solitary wave solution corresponding to the separatrix shown in Fig. 5. Shown is $u_1^2+u_2^2=|f_\pm|^2$ as a function of position.

As a final point we note that it has been shown that for a shallow grating a one-band description as in Sec. III A can be obtained from the two-band description as in Sec. III B [30] in the limit that $\tilde{\Delta}\to\sigma$. This limiting behavior can be recognized in solution (55): as $\tilde{\Delta}_1\to 2\sigma$, $\tilde{\Delta}_2\to 0$. Then $u_1\to 0$ and u_2 takes on a hyperbolic secant shape, consistent with the one-soliton solutions to Eq. (28).

V. DISCUSSION AND CONCLUSION

We have applied an approach, originally developed for treating deep uniform nonlinear gratings, to deep nonlinear SSG's, leading to a set of SCME's. Since our method is based upon the Bloch functions of the SSG's its validity is quite general. It represents a generalization of results obtained by others [2,8] in the limit of shallow, linear SSG's. We have shown that the SCME's for deep SSG's are simple generalizations of the coupled mode equations for uniform gratings, by the additon of some extra terms. Now often the extra terms obtained for deep SSG's are quite small: in this case a deep SSG thus behaves the same as a shallow grating. Thus, we may conclude that in analogy to grating solitons in uniform gratings, solitary wave solutions (Rowland ghost solitons) can propagate through SSG's. These solitary waves can be excited by a sufficiently strong external pulse incident on the SSG, as has been demonstrated in recent experiments in optical fibers [5]. For the case in which the new terms in the SCME's for deep SSG's cannot be neglected, we have proven the existence of stationary solitary solutions. We would expect that in this case more general solutions, such as traveling solitary wave solutions and stationary and traveling dark solutions, also exist.

As mentioned in the preceding paragraph, SSG's often behave like shallow uniform gratings. However, it should be noted that this resemblance fails at the two boundaries of an SSG: in a shallow uniform grating the envelope functions are continuous over each such interface, while for SSG's the interface conditions are somewhat more complicated, and involve the Bloch functions. This difference is not important when considering solitary wave solutions in inifinite media, but do play an important role when, for example, calculating the reflection spectrum of a SSG [15].

Our treatment shows that the criterion commonly used in the literature for a SSG to be shallow is overly restrictive, and that simple results can be obtained under somewhat more general conditions [see Eqs. (A13) and the discussion following it]. Under these more general conditions the Rowland ghost gaps are not equally spaced in detuning, especially if ℓ is not too large [Eq. (17)]; this contrasts standard results in which the Rowland ghost gaps are taken to be equally spaced [3,8]. Moreover, we show in the Appendix that the size of a Rowland ghost gap is not simply given by the associated Fourier component of the SSG [Eqs. (A13)]. The differences occur because a SSG can be considered to be a perturbed *uniform* grating, which has a curved dispersion relation (see Fig. 2); equally spaced Bragg resonances only occur when the underlying dispersion relation is taken to be a straight line.

Possible generalizations of our work would involve start-

ing from the coupled mode equations for a *deep* uniform grating, rather than those for a shallow one as we did here [Eqs. (4)]. One could surmise that if one could show that these also lead to SCME's such as Eqs. (42) (of course with different coefficients), this would imply the existence of a hierarchy, where at every length scale a similar set of equations applies. It would also imply that Eqs. (42) are the most general set of equations that apply to periodic media with a nonlinearity, and that any such structure supports solitary wave solutions at every scale.

In conclusion, we have presented a general theory of SSG's, leading to a set of SCME's (42). These reduce to well-known results in appropriate limits, and have an appealing resemblance to the standard coupled mode equations for uniform gratings. We have also shown that in the most general case the SCME's possess stationary solitary wave solutions, and we surmise that these are members of a more general set which can travel through the SSG unimpeded.

ACKNOWLEDGMENTS

The authors are grateful to Ben Eggleton and John Sipe for many discussions regarding SSG's, and James Yardley for proving inequality (40). This research was supported by the Australian Research Council.

APPENDIX A: FOURIER METHOD FOR CALCULATING BLOCH FUNCTIONS

In Sec. II we showed that the Bloch functions for a metagrating are solutions to eigenvalue problem (13). Here we outline a method which provides numerical solutions to the eigenvalue problem. We also give explicit expressions for the Bloch functions for shallow SSG's.

Since all the functions of interest in Eq. (13) have periodic components [e.g., see Eq. (15)], following a standard procedure in condensed matter physics [21], we can make the following expansions:

$$\kappa(x)=\sum_{\ell}\ \kappa_{\ell}e^{i\frac{2\pi\ell}{\Lambda}x}, \tag{A1}$$

$$\delta(x)=\sum_{\ell}\ \delta_{\ell}e^{i\frac{2\pi\ell}{\Lambda}x}, \tag{A2}$$

$$\psi_{+}(x,t)=\left(\sum_{\ell}\ a_{+,\ell}e^{i\frac{2\pi\ell}{\Lambda}x}\right)e^{ikx}, \tag{A3}$$

$$\psi_{-}(x,t)=\left(\sum_{\ell}\ a_{-,\ell}e^{i\frac{2\pi\ell}{\Lambda}x}\right)e^{ikx}, \tag{A4}$$

where the only unknowns are the coefficients $a_{\pm,\ell}$. Note that since $\kappa(x)$ and $\delta(x)$ are real functions [Eq. (5)] we must have $\kappa_{-\ell}=\kappa_{\ell}^{\star}$, and similarly for δ. In terms of expansions (A1)–(A4), Eqs. (13) can be written as

$$\sum_{\ell}\left[\left(k+\frac{2\pi\ell}{\Lambda}-\Delta\right)a_{+,\ell}-\sum_{n}\ \delta_{\ell-n}a_{+,n}-\sum_{n}\ \kappa_{\ell-n}a_{-,n}\right]e^{i\frac{2\pi\ell}{\Lambda}x}=0,$$

$$\sum_{\ell}\left[\left(-k-\frac{2\pi\ell}{\Lambda}-\Delta\right)a_{-,\ell}-\sum_{n}\ \delta_{\ell-n}a_{-,n}-\sum_{n}\ \kappa_{\ell-n}a_{+,n}\right]e^{i\frac{2\pi\ell}{\Lambda}x}=0. \tag{A5}$$

The transformation from Eq. (13) to Eqs. (A5) can be thought of as being equivalent to changing from a coordinate representation to a momentum representation in quantum mechanics. Since the exponentials in the sums in Eq. (A5) are orthogonal, the only way the sums can be zero is if all the coefficients vanish. Thus for each integer ℓ we have the following *two* equations:

$$\left(+k+\frac{2\pi\ell}{\Lambda}-\delta_0-\Delta\right)a_{+,\ell}-\sum_{n;n\neq\ell}\ \delta_{\ell-n}a_{+,n}-\sum_{n}\ \kappa_{\ell-n}a_{-,n}=0,$$

$$\left(-k-\frac{2\pi\ell}{\Lambda}-\delta_0-\Delta\right)a_{-,\ell}-\sum_{n;n\neq\ell}\ \delta_{\ell-n}a_{-,n}-\sum_{n}\ \kappa_{\ell-n}a_{+,n}=0. \tag{A6}$$

This infinite set is equivalent to the eigenvalue problem

$$A\vec{a}=\Delta\vec{a}, \tag{A7}$$

where A is the infinite Hermitian matrix consisting of

$$A_{i,j}=\begin{cases}\begin{bmatrix}k+\frac{2\pi j}{\Lambda}-\delta_0 & -\kappa_0\\ -\kappa_0 & -k-\frac{2\pi j}{\Lambda}-\delta_0\end{bmatrix}, & i=j\\ \begin{bmatrix}\delta_{j-i} & \kappa_{j-i}\\ \kappa_{j-i} & \delta_{j-i}\end{bmatrix}, & i\neq j\end{cases} \tag{A8}$$

and $\vec{a}$ is the column vector with elements

$$(\ldots,a_{+,-1},a_{-,-1},a_{+,0},a_{-,0},a_{+,1},a_{-,1}\ldots). \tag{A9}$$

Equation (A7) shows that the only effect of the zeroth-order Fourier component of $\delta(x)$ is to shift the detunings of all the eigenvalues uniformly, as, for example, in Eq. (8). The ''central'' region of matrix A is

$$\begin{pmatrix}
-\delta_0-k+\frac{4\pi}{\Lambda} & -\kappa_{-1} & -\delta_{-1} & -\kappa_{-2} & -\delta_{-2} & -\kappa_{-3} & -\delta_{-3} & -\kappa_{-4} \\
-\kappa_1 & -\delta_0+k-\frac{2\pi}{\Lambda} & -\kappa_0 & -\delta_{-1} & -\kappa_{-1} & -\delta_{-2} & -\kappa_{-2} & -\delta_{-3} \\
-\delta_1 & -\kappa_0 & -\delta_0-k+\frac{2\pi}{\Lambda} & -\kappa_{-1} & -\delta_{-1} & -\kappa_{-2} & -\delta_{-2} & -\kappa_{-3} \\
-\kappa_2 & -\delta_1 & -\kappa_1 & -\delta_0+k & -\kappa_0 & -\delta_{-1} & -\kappa_{-1} & -\delta_{-2} \\
-\delta_2 & -\kappa_1 & -\delta_1 & -\kappa_0 & -\delta_0-k & -\kappa_{-1} & -\delta_{-1} & -\kappa_{-2} \\
-\kappa_3 & -\delta_2 & -\kappa_2 & -\delta_1 & -\kappa_1 & -\delta_0+k+\frac{2\pi}{\Lambda} & -\kappa_0 & -\delta_{-1} \\
-\delta_3 & -\kappa_2 & -\delta_2 & -\kappa_1 & -\delta_1 & -\kappa_0 & -\delta_0-k-\frac{2\pi}{\Lambda} & -\kappa_{-1} \\
-\kappa_4 & -\delta_3 & -\kappa_3 & -\delta_2 & -\kappa_2 & -\delta_1 & -\kappa_1 & -\delta_0+k+\frac{4\pi}{\Lambda}
\end{pmatrix}. \tag{A10}$$

We have thus transformed the coupled differential equations (13) into matrix equation (A7), where A is an infinite Hermitian matrix. The eigenvalues of A correspond to those of Eq. (13), and thus give the frequencies of the Bloch functions. The eigenvectors of A, via Eqs. (A9), (A3), and (A4), give the Bloch functions.

It may not be immediately clear that solving the eigenvalue problem for an infinite Hermitian matrix is an improvement over solving Eq. (13). However, this approach has a number of advantages. Importantly we can truncate the matrix A and find the eigenvalues and eigenvectors numerically. This is useful if we are interested in only the first few eigenvalues, corresponding to the location of the first few Rowland ghosts, as the inclusion of higher-order Fourier coefficients is unlikely to alter the results significantly. To calculate the band diagram in Fig. 3 and the Bloch functions in Fig. 4 we approximated A by a 200×200 Hermitean matrix. In Fig. 3 only 15 bands can be seen, although by solving the eigenvalue problem for a 200×200 matrix we obtain 200 bands. Choosing an appropriate size for the matrix is a tradeoff between accuracy and speed. The larger the matrix, the more accurate the eigenvalues, but at the cost of a longer calculation. The required size of the matrix also depends on the SSG profile. For a SSG as in Fig. 1, which has discontinuities, the magnitude of the Fourier components decreases as $1/|n|$, where n is the order; clearly, in this case the required size of the matrix is larger than for SSG's without discontinuities, where the Fourier components' magnitude decreases more rapidly.

Results for the weak SSG limit

As mentioned in Sec. II B, there is some ambiguity as to how to define a shallow SSG. Jayaraman *et al.* [8], for example, implicitly define a SSG to be shallow if all Fourier components including $n=0$ satisfy inequality (20). However, this would lead to the conclusion that *any* uniform grating, which can always be considered to be a SSG with infinitesimal periodic perturbation with arbitrary period, is a *deep* SSG. For this reason one could argue for the exclusion of the dc component of κ from inequalities (20). Below we adopt this latter definition, as results for the more restrictive criterion of Jayaraman *et al.* [3,8] follow as a special case.

From the general matrix (A10) it is easy to obtain results valid in the weak SSG limit. In the shallow SSG limit, then, the δ_ℓ and κ_ℓ ($\ell\neq0$) are taken to be small, and only first-order contributions in these parameters are included. Consider first values of k away from the edge and the center of the Brillouin zone ($k\neq0,\pi/\Lambda$). Then all diagonal elements of matrix (A10) differ, and the small parameters δ_ℓ and κ_ℓ only contribute to second order to the eigenvalues. Consequently, we ignore these small parameters, which only leaves the $i=j$ blocks of Eq. (A8) in matrix (A10). The diagonalization of these gives rise to the dispersion relation given by the solid line in Fig. 2. Thus for values of k away from the center and edges of the Brillouin zone the dispersion curve for a shallow SSG is the same as that for a uniform grating (see Sec. II B).

We now consider the edge and the center of the Brillouin zone. The situation is now more complicated than that discussed in the paragraph above because the diagonal elements of matrix (A10) are now two-by-two the same. For this reason the small off-diagonal elements of matrix (A10) contribute linearly to the eigenvalues, and thus they cannot be neglected. Retaining only first-order contributions, it can be seen by inspection that matrix (A10) can be block-diagonalized by simply interchanging rows and columns; each block is a 4×4 submatrix. The submatrices can be written as

$$\begin{bmatrix} -\delta_0 - D_\ell \cos\varphi_\ell & -D_\ell \sin\varphi_\ell & -\delta_\ell & -\kappa_{-\ell} \\ -D_\ell \sin\varphi_\ell & -\delta_0 + D_\ell \cos\varphi_\ell & -\kappa_{-\ell} & -\delta_\ell \\ -\delta_\ell & -\kappa_\ell & -\delta_0 + D_\ell \cos\varphi_\ell & -D_\ell \sin\varphi_\ell \\ -\kappa_\ell & -\delta_\ell & -D_\ell \sin\varphi_\ell & -\delta_0 - D_\ell \cos\varphi_\ell \end{bmatrix}, \tag{A11}$$

where ℓ is a nonzero integer, and

$$D_\ell \cos\varphi_\ell = \frac{\ell\pi}{\Lambda},$$

$$D_\ell \sin\varphi_\ell = \kappa_0. \tag{A12}$$

Even values of ℓ occur at $k=0$, while odd values occur at $k=\pi/\Lambda$. The submatrices (A11) can easily be diagonalized; the four eigenvalues are

$$\Delta = -\delta_0 + D_\ell \pm |\kappa_\ell - \delta_\ell \sin\varphi_\ell|,$$

$$\Delta = -\delta_0 - D_\ell \pm |\kappa_\ell + \delta_\ell \sin\varphi_\ell|. \tag{A13}$$

This means that, for shallow SSG's, the Rowland ghost gaps are centered about the detunings D_ℓ [Eq. (17)], and have widths $2|\kappa_\ell \pm \delta_\ell \sin\varphi_\ell|$. The more restrictive results of Jayaraman *et al.* [8] are obtained as $\kappa_0 \to 0$, so that $D_\ell = \ell\pi/\Lambda$ [Eq. (17)], and $\sin\varphi_\ell = 0$ [Eq. (A12)].

Thus far we have only used the eigenvalues of the submatrices (A11). Via Eqs. (A3) and (A4) the eigenvectors immediately lead to the Bloch functions. Thus using normalization (24) and convention (23), the Bloch function at $\Delta = -\delta_0 + D_\ell + |\kappa_\ell - \delta_\ell \sin\varphi_\ell|$, at the top of Rowland ghost gap ℓ, is given by

$$\psi_+(x) = \frac{i}{\sqrt{2\Lambda}}(\sin\varphi_\ell e^{-i\Theta_\ell} + \cos\varphi_\ell e^{+i\Theta_\ell}),$$

$$\psi_-(x) = -\frac{i}{\sqrt{2\Lambda}}(\cos\varphi_\ell e^{-i\Theta_\ell} + \sin\varphi_\ell e^{+i\Theta_\ell}), \tag{A14}$$

where

$$\Theta_\ell = \frac{\pi\ell}{\Lambda} + \frac{1}{2}\arg(\kappa_\ell). \tag{A15}$$

Similarly, at $\Delta = -\delta_0 + D_\ell - |\kappa_\ell - \delta_\ell \sin\varphi_\ell|$, at the bottom of Rowland ghost gap ℓ,

$$\psi_+(x) = \frac{1}{\sqrt{2\Lambda}}(\sin\varphi_\ell e^{-i\Theta_\ell} - \cos\varphi_\ell e^{+i\Theta_\ell}),$$

$$\psi_-(x) = \frac{1}{\sqrt{2\Lambda}}(-\cos\varphi_\ell e^{-i\Theta_\ell} + \sin\varphi_\ell e^{+i\Theta_\ell}). \tag{A16}$$

Note that both Bloch functions satisfy Eq. (23), as required. Finally, the Bloch functions of the photonic band gap centered around $\Delta = -\delta_0 - D_\ell$ can be found from Eqs. (A14) and (A16) by replacing φ_ℓ by $\varphi_\ell + \pi/2$.

[1] W.H. Loh, M.J. Cole, M.N. Zervas, S. Barcelos, and R.I. Laming, Opt. Lett. **20**, 2051 (1995).

[2] P.St.J. Russell, J. Appl. Phys. **59**, 3344 (1986).

[3] B.J. Eggleton, P.A. Krug, L. Poladian, and F. Ouellette, Electron. Lett. **30**, 1620 (1994).

[4] M. Ibsen, B.J. Eggleton, M.G. Sceats, and F. Ouellette, Electron. Lett. **31**, 37 (1995).

[5] B.J. Eggleton, C.M. de Sterke, and R.E. Slusher, Opt. Lett. **21**, 1223 (1996).

[6] F. Ouellette, P.A. Krug, and R. Pasman, Opt. Fiber Technol. **2**, 281 (1996).

[7] G.W. Stroke, in *Optical Instruments*, edited by S. Flügge, Encyclopedia of Physics Vol. XXIX (Springer-Verlag, New York, 1967), Chap. 4.

[8] V. Jayaraman, Z.-M. V. Chuang, and L.A. Coldren, IEEE J. Quantum Electron. **29**, 1824 (1992).

[9] H. Ishii, H. Tanobe, F. Kano, Y. Tohmori, Y. Kondo, and Y. Yoshikuni, IEEE J. Quantum Electron. **32**, 433 (1996).

[10] F. Ouellette, P.A. Krug, T. Stephens, G. Dhosi, and B.J. Eggleton, Electron. Lett. **31**, 899 (1995).

[11] D. Marcuse, *Theory of Dielectric Optical Waveguides*, 2nd ed. (Academic, San Diego, 1991).

[12] D.G. Salinas, C.M. de Sterke, and J.E. Sipe, Opt. Commun. **111**, 105 (1994).

[13] C.M. de Sterke, D.G. Salinas, and J.E. Sipe, Phys. Rev. E **54**, 1969 (1996).

[14] P.St.J. Russell, J. Mod. Opt. **38**, 1599 (1991).

[15] C.M. de Sterke and N.G.R. Broderick, Opt. Lett. **20**, 2039 (1995).

[16] N.G.R. Broderick, C.M. de Sterke, and B.J. Eggleton, Phys. Rev. E **52**, R5788 (1995).

[17] J.E. Sipe, L. Poladian, and C.M. de Sterke, J. Opt. Soc. Am. A **11**, 1307 (1994).

[18] H.G. Winful and G.D. Cooperman, Appl. Phys. Lett. **40**, 298 (1982).

[19] C.M. de Sterke and J.E. Sipe, *Gap Solitons*, in Progress in Optics Vol. XXXIII, edited by E. Wolf (North-Holland, Amsterdam, 1994), pp. 203–260.

[20] J.M. Ziman, *Principles of the Theory of Solids*, 2nd ed. (Cambridge University Press, Cambridge, 1972).

[21] C. Kittel, *Introduction to Solid State Physics*, 5th ed. (Wiley, New York, 1976), Chap. 7.

[22] C.M. de Sterke and J.E. Sipe, Phys. Rev. A **38**, 5149 (1988).

[23] M. Born and E. Wolf, *Principles of Optics*, 6th ed. (Pergamon, Oxford, 1980), Appendix VIII.

[24] C.M. de Sterke, Phys. Rev. E **48**, 4136 (1993).
[25] Y.S. Kivshar and N. Flytzanis, Phys. Rev. A **46**, 7972 (1992).
[26] W. Chen and D. L. Mills, Phys. Rev. Lett. **58**, 160 (1987).
[27] A.B. Aceves and S. Wabnitz, Phys. Lett. A **141**, 37 (1989).
[28] B.J. Eggleton, R.E. Slusher, C.M. de Sterke, P.A. Krug, and J.E. Sipe, Phys. Rev. Lett. **76**, 1627 (1996).
[29] J. Feng and F. Kneubühl, IEEE J. Quantum. Electron. **29**, 590 (1993).
[30] C.M. de Sterke and J.E. Sipe, Phys. Rev. A **42**, 550 (1990).